In situ micro-Raman spectroscopy to investigate pitting corrosion product of 1024 mild steel in phosphate and bicarbonate solutions containing chloride and sulfate ions

S. SIMARD[1],*, M. ODZIEMKOWSKI[2], D.E. IRISH[3], L. BROSSARD[4] and H. MÉNARD[1]

[1]*Département de Chimie, Université de Sherbrooke, Sherbrooke (Québec), Canada J1K 2R1*
[2]*Department of Earth Sciences, University of Waterloo, Waterloo (Ontario), Canada N2L 3G1*
[3]*Department of Chemistry, University of Waterloo, Waterloo (Ontario), Canada N2L 3G1*
[4]*Institut de Recherche d'Hydro-Québec (IREQ), 1800 boul. Lionel-Boulet, Varennes (Québec), Canada J3X 1S1*

Abstract

The nature of the corrosion products generated by localized attack on 1024 mild steel have been investigated in the presence of chloride and/or sulfate ions in bicarbonate and phosphate aqueous solutions. A spectroelectrochemical cell was used for *in situ* measurements of the Raman spectra of the corrosion products generated during pitting. These products were identified as the so-called green rust compounds. The assignment of the hydroxyl groups in green rust is confirmed by isotopic substitution. The composition of the green rust generated in bicarbonate or phosphate solution containing chloride and/or sulfate ions has been determined. A correlation between the green rust composition and the electrochemical behaviour after the initiation of pitting has been noted and discussed.

1. Introduction

Pitting corrosion is observed in a wide variety of metals, alloys and environments [1–3]. In slightly alkaline (pH 9) bicarbonate and phosphate aqueous solutions, iron and mild steel can become covered by a thin oxide passive film [4–15]; this film is subject to breakdown in the presence of aggressive ions such as chloride above a given electrode potential, i.e., the breakdown potential [16–19]. After the pit initiation on 1024 mild steel, it is reported that both the electrochemical behaviour and the morphology of the precipitate generated during pitting are dependent on the solution composition (i.e., bicarbonate or phosphate) [18]. Such differences suggest that the nature of the corrosion product covering the pits is linked to the nature of the ions in the solution.

Some authors have reported that the electrodissolution of iron in the aqueous solutions may lead to the formation of a thick unstable colloidal hydroxy salt layer called green rust (GR) [20]. The structure of green rust is composed of Fe(II), Fe(III), hydroxyl ions, and nonhydroxyl ions, which may consist of sulfates, halides, nitrates or carbonates; even organic anions may be involved [21]. The chemical composition of the green rust and its stoichiometry can vary depending on the ambient conditions and on the nature of the anions in solution [21–24]. The existence of two types of green rust (GR1 and GR2) has been suggested depending on the nature of the existing anions. Some examples of the chemical formulae reported in the literature are $3Fe(OH)_2 \cdot Fe(OH)_2Cl \cdot nH_2O$ for GR1 and $4Fe(OH)_2 \cdot FeOOH \cdot FeSO_4 \cdot nH_2O$ for GR2. The chloride-containing GR1 can be transformed into sulfate containing GR2 (depending on the sulfate/chloride ratio) through the following pathway [25]:

$$Fe(OH)_2 \rightarrow GR1 \rightarrow GR2 \rightarrow \alpha \text{ or } \gamma - FeOOH$$

In many studies, green rust was synthetized by precipitation and its structure has been investigated with X-ray diffraction, Mössbauer and Raman spectroscopies of the resulting filtrate [21, 25–28]. In an earlier paper [29], it was reported that the structure of the green rust in the form of a corrosion product is different from those associated with GR1 and GR2 generated by synthesis. Consequently, for studies aimed at better understanding the corrosion mechanisms, the first step consists in characterizing the green rust generated by a corrosion phenomenon. In both cases, the conditions under which the precipitate is formed are probably quite different, that is, the solution composition in the vicinity of the corroding metal surface, especially during pitting, may be quite different from the bulk solution.

*Present address: Département de Biologie, Chimie et Sciences de la Santé, Université du Québec à Rimouski, Rimouski (Québec), Canada G5L 3A1

The surface oxide film formed on stainless steel in sodium hydroxide solution containing chloride ions was recently studied and green rust was identified under *ex situ* conditions [20]. Since the corrosion product is unstable when in contact with air, the present study was performed entirely *in situ* using Raman spectroscopy for the surface analysis. Raman spectroscopy is powerful because of its *in situ* possibilities for molecular analysis in aqueous media without any significant effect from a high roughness factor. The interest for this technique is enhanced by the use of an optical microscope which gives precise spatial resolution and allows very small spots to be selected for analysis. Raman spectroscopy was recently used for the *in situ* identification of green rust in solutions simulating ground water [30].

The present work is devoted to the *in situ* analysis of the solids formed over the pits in slightly alkaline aqueous bicarbonate and phosphate solutions during pitting and electrodissolution of 1024 mild steel.

2. Experimental details

The electrochemical experiments were performed in both a spectroelectrochemical cell and electrochemical cell at room temperature. The spectroelectrochemical cell is described in Figure 1. The working electrodes consisted of stationary and rotating 1024 mild steel disc electrodes having a 4 mm diameter (surface area = 0.126 cm^2). The discs were prepared from a steel rod set in a Kel-F holder. The composition of 1024 mild steel is given in [8]. Before each measurement, the working electrode was ground with 600 and 3/0 emery paper and polished using 1 μm and 0.05 μm alumina suspensions before rinsing with deionized water. The stationary electrode was used for the experiments in the spectroelectrochemical cell.

The rotating disc electrode was preferred in order to promote the homogeneity of the solution near the electrode surface; an H-shaped electrochemical cell described in [8] was used. The tip of the electrode was removable to allow its transfer to a spectroscopic cell filled with the same solution as the one in the electrochemical cell. During the transfer, a drop of solution was kept on the electrode surface to avoid any direct contact with air. During a first set of experiments, it was observed that the spectra of the corrosion products recorded in the electrochemical cell were exactly the same as those obtained in the spectroelectrochemical cell for which the electrode transfer was avoided. This indicates that the transfer procedure of the rotating electrode tip was acceptable; that is, it had no effect on the composition of the corrosion product. The auxiliary electrode was a platinum electrode and the reference was a calomel electrode. All solutions were prepared with deionized water or D$_2$O 99% CIL Isotope and BDHassured® or Anachemia® analytical reagent grade chemicals. All the experiments were performed at room temperature, pH 9, and in deaerated solutions under a N$_2$ stream.

The film breakdown was induced by a linear potential sweep in the anodic direction and the potential scan was stopped at a potential slightly more positive than that of pit nucleation (E_{pn}). Under such conditions, $a \sim 50$ μm pit was formed and it was covered by a corrosion product.

The spectra of the corrosion products were obtained with a Renishaw 1000 Raman system with CCD detector. Excitation was achieved using the 632.8 nm line of a Melles Griot 35 mW HeNe laser. The laser was focused on a 2 μm spot of corrosion product *in situ*, using an Olympus microscope with an objective lens magnification of 50 and backscattered Raman light was efficiently collected by the same lens.
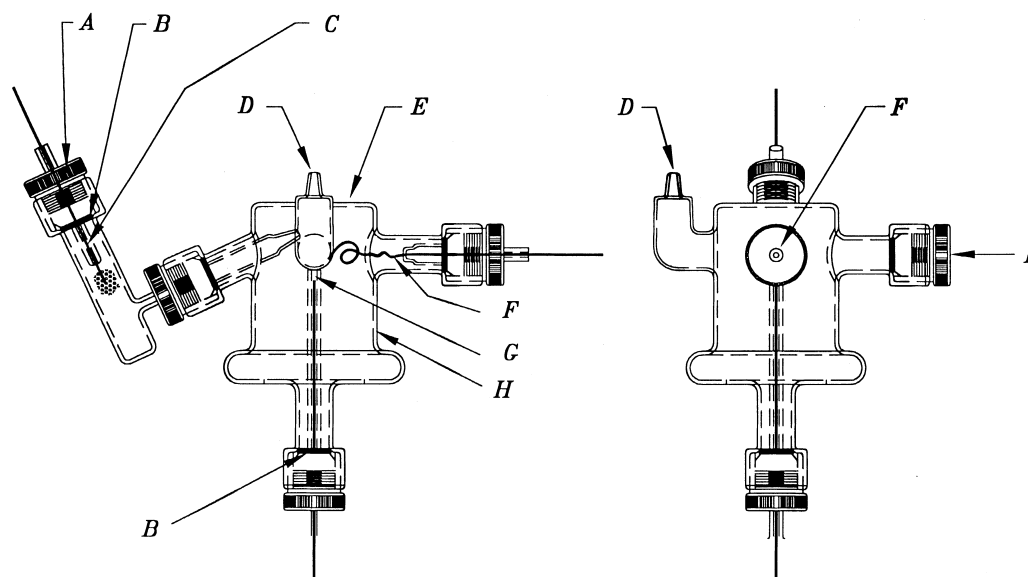

Fig. 1. Spectroelectrochemical cell testing apparatus: (A) cap, (B) O-ring, (C) Ag/AgCl reference electrode, (D) overflow hole, (E) optical window, (F) platinum counter electrode, (G) 1024 mild steel electrode, (H) glass and (I) injection port.

3. Results and discussion

3.1. *Potentiodynamic behaviour and corrosion product electrogeneration*

The potentiodynamic polarization curves recorded for bicarbonate solutions ($dE/dt = 2$ mV s^{-1}) are illustrated in Figure 2: (a) for a 0.1 M NaHCO$_3$ solution, (b) for a 0.1 M NaHCO$_3$ + 0.15 M NaCl solution and (c) for a 0.1 M NaHCO$_3$ solution with preanodization prior to the potential scan and the addition of NaCl to the solution. The potential scan was started at −0.835 V because the rate of hydrogen evolution is negligible and the potential reversal was 0.9 V (just before the beginning of the transpassive dissolution). The potentiodynamic trace for 0.1 M NaHCO$_3$ solution is characterized by a large oxidation peak located at −0.65 V, and a passive region extending over 1.4 V. The oxidation current peak at −0.65 V, reaching a maximum of 0.12 mA cm^{-2}, is related to the electrodissolution of Fe(0) to Fe(II) aqueous species and carbonate/bicarbonate species are involved in the reaction [8]. The cathodic section of the potentiodynamic curve displays a small reduction current peak at −0.75 V, which is ascribed to the reduction of the passive oxide film [8].

The potentiodynamic trace is practically the same up to about −0.14 V, with the addition of 0.15 M NaCl (Figure 2(b)). At this potential, the increase of anodic current is noticed. The increase is linked to the film breakdown and formation of pits which permit local iron active dissolution and the formation of a porous precipitate covering the pit. The local active dissolution of iron through this precipitate has been previously noticed in such media using a rotating ring disk electrode [19].

The picture is different for preanodization (Figure 2(c)). The electrode was preanodized for 45 min at −0.4 V in 0.1 M NaHCO$_3$ solution and, immediately after, a concentrated chloride solution was injected into the electrochemical cell; the potential scan in the anodic direction was started (Figure 2(c)). At the beginning of the scan, a small residual anodic current was noticed until the passive film breakdown at about −0.14 V.

The potentiodynamic polarization curves recorded for iron in 0.1 M NaHCO$_3$ + 0.1 M Na$_2$SO$_4$ (Figure 3(a)) and 0.1 M NaHCO$_3$ + 0.1 M Na$_2$SO$_4$ + 0.15 M NaCl (Figure 3(b)) were characterized by an anodic current peak located at −0.65 V, with a maximum of 0.2 mA cm^{-2}, that is, 0.08 mA cm^{-2} higher than in the absence of Na$_2$SO$_4$. This evidence suggests that the sulfate ions are also involved in the active dissolution process of iron [8].

In bicarbonate solution containing sulfate ions, a passive film breakdown is observed which indicates that sulfate is aggressive under such conditions. The breakdown potential is located practically at the same value as in the presence of chloride ions (Figure 2(b)). In a solution containing 0.1 M NaHCO$_3$ + 0.1 M

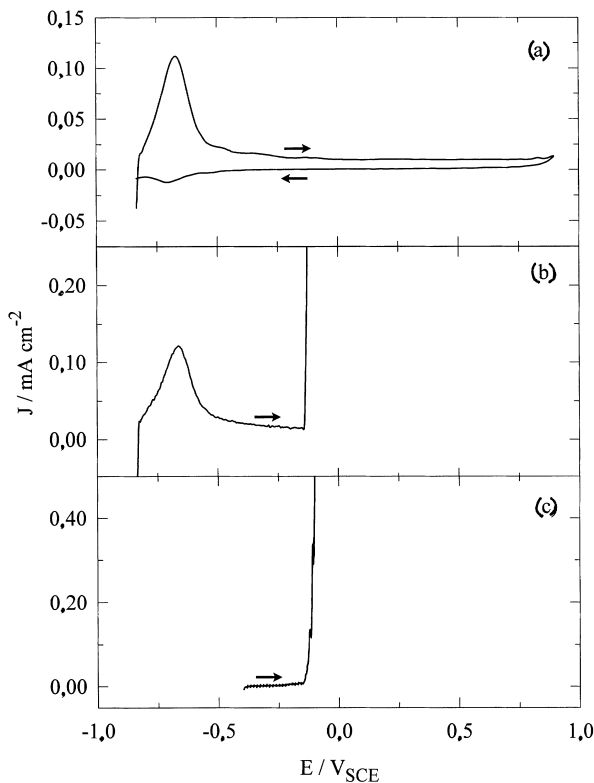*Fig. 2.* Potentiodynamic anodic polarization curves for 1024 mild steel rotating electrode in: (a) 0.1 M NaHCO$_3$, (b) 0.1 M NaHCO$_3$ + 0.15 M NaCl, (c) 0.1 M NaHCO$_3$ following 45 min passivation and + 0.15 M NaCl at the beginning of the sweep. (ω = 1000 rpm, dE/dt = 2 mV s^{-1}).

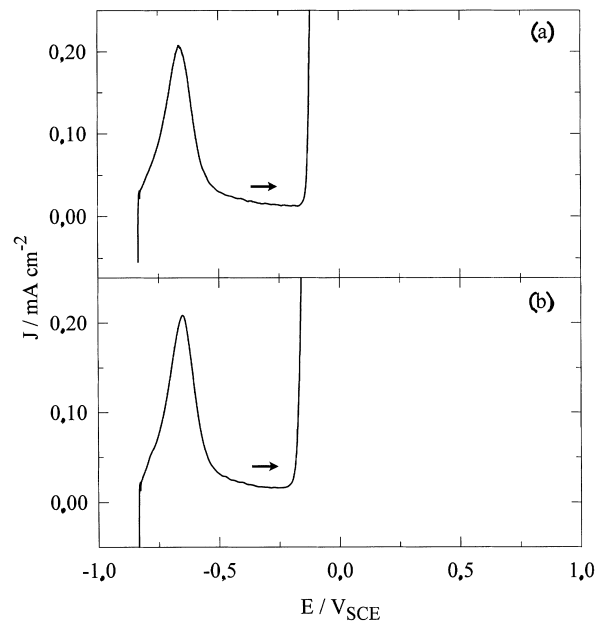*Fig. 3.* Potentiodynamic anodic polarization curves for 1024 mild steel rotating electrode in: (a) 0.1 M NaHCO$_3$ + 0.1 M Na$_2$SO$_4$ (b) 0.1 M NaHCO$_3$ + 0.1 M Na$_2$SO$_4$ + 0.15 M NaCl. (ω = 1000 rpm, dE/dt = 2 mV s^{-1}).

Na$_2$SO$_4$ + 0.15 M NaCl (Figure 3(b)), the shift of the breakdown potential in the cathodic direction is about 50 mV. This can be explained by the fact that the higher total concentration of aggressive anions decreases the breakdown potential [30] and both chloride and sulfate ions promote the localized film breakdown. The localized attack takes the form of pits covered by a precipitate in all bicarbonate solutions containing chloride and/or sulfate ions. Even in the presence of the precipitate, the pit continues to grow without significant inhibition of the corrosion process.

Figure 4 shows the potentiodynamic polarization curves obtained in different solutions containing phosphate: 0.1 M Na$_2$HPO$_4$ for Figure 4(a), and 0.1 M Na$_2$HPO$_4$ + 0.15 M NaCl for Figure 4(b) and (c). The anodic peak current located at -0.6 V is related to the active dissolution of mild steel and its maximum current is 0.08 mA cm^{-2} in the presence of phosphate ions alone, which is lower than when in the bicarbonate media. A passive region is observed over 1.4 V at more positive potentials than the primary passive potential. The cathodic section of the trace shows a small reduction peak which is linked to the passive film reduction [18].

The potentiodynamic curve obtained in 0.1 M Na$_2$HPO$_4$ + 0.15 M NaCl solution is illustrated in Figure 4(b). The initiation of the passive film breakdown occurs at a potential of about 0.05 V, where some current oscillations occur. A recent paper shows that the morphology of the precipitate generated during the localized attack is different in the presence of phosphate ions than in the presence of bicarbonate ions [18]. It is reported that in the presence of the precipitate generated in the phosphate solution containing chloride anions slowed down the corrosion process. Such behaviour was not observed in the bicarbonate media containing chloride anions.

The potentiodynamic curve given in Figure 4(c) was obtained in a phosphate solution after preanodization for 45 min in 0.1 M Na$_2$HPO$_4$ following the same procedure as for Figure 2(c). Some small anodic current oscillations start at a potential close to 0 V which indicates the beginning of the metastable oxidation process. The more anodic the potential, the higher the magnitude of the current oscillations.

The voltammograms for aqueous phosphate solutions containing sulfate ions are given in Figure 5. The voltammogram of Figure 5(a) was obtained in 0.1 M Na$_2$HPO$_4$ + 0.1 M Na$_2$SO$_4$. The electrochemical behaviour is practically the same as in the phosphate solution free of dissolved Na$_2$SO$_4$ (Figure 4(a)). Thus, we conclude that in aqueous phosphate solutions and under the experimental conditions mentioned above, the sulfate ions are nonaggressive and do not induce passive film breakdown. The effect of sulfate ions in the bicarbonate solution acts in the opposite direction by promoting the localized attack of mild steel (Figure 3(a)).
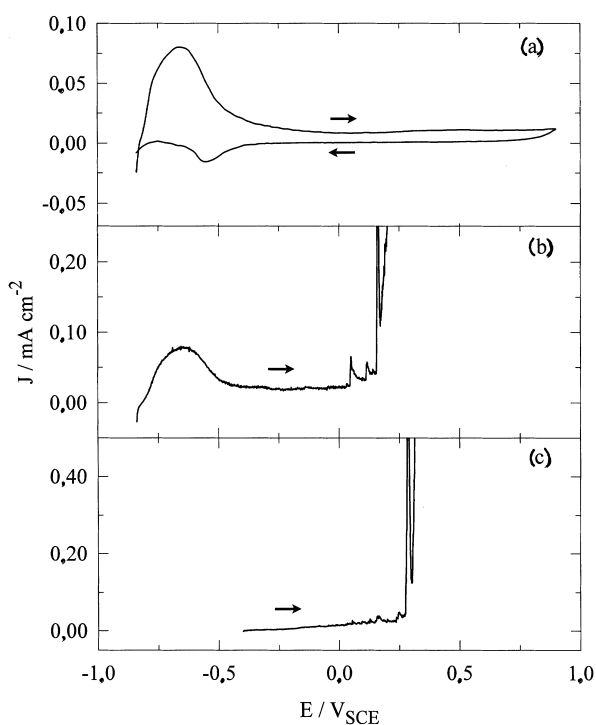

Fig. 4. Potentiodynamic anodic polarization curves for 1024 mild steel rotating electrode in: (a) 0.1 M Na$_2$HPO$_4$, (b) 0.1 M Na$_2$HPO$_4$ + 0.15 M NaCl, (c) 0.1 M Na$_2$HPO$_4$ following 45 min passivation and + 0.15 M NaCl at the beginning of the sweep. (ω = 1000 rpm, dE/dt = 2 mV s^{-1}).
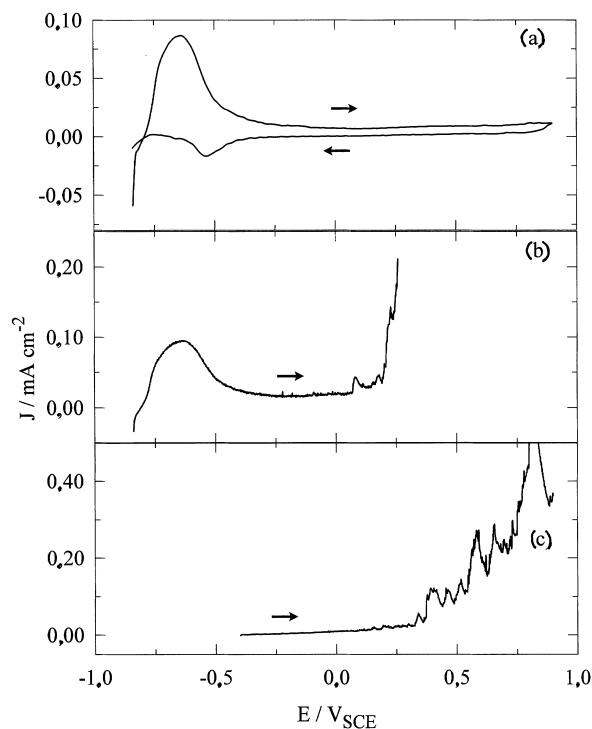

Fig. 5. Potentiodynamic anodic polarization curves for 1024 mild steel rotating electrode in: (a) 0.1 M Na$_2$HPO$_4$ + 0.1 M Na$_2$SO$_4$, (b) 0.1 M Na$_2$HPO$_4$ + 0.1 M Na$_2$SO$_4$ + 0.15 M NaCl, (c) 0.1 M Na$_2$HPO$_4$ + 0.1 M Na$_2$SO$_4$ following 45 min passivation and + 0.15 M NaCl at the beginning of the sweep. (ω = 1000 rpm, dE/dt = 2 mV s^{-1}).

Figure 5(b) and (c) show the effect of the presence of chloride anions in the phosphate/sulfate solution (i.e., 0.1 M Na$_2$HPO$_4$ + 0.1 M Na$_2$SO$_4$ + 0.15 M NaCl). A breakdown potential at about 0.07 V is noticed (Figure 5(b)) and the electrochemical behaviour is quite similar to that shown in Figure 4(b). The passive film breakdown occurs practically at the same potential; however, the current oscillations are less sharp in the presence of sulfate ions with chloride ions than in the presence of chloride ions without any sulfate in the phosphate solution (Figure 4(b)). The difference in the shape of the current oscillations is shown off by the potentiodynamic curve obtained with the preanodized electrode (Figure 5(c)). The above observations suggest that the chloride anions initiate the film breakdown but the sulfate anion may be involved in the metastable electrooxidation process.

3.2. Spectroscopic data

The *in situ* Raman spectrum (200–700 cm^{-1}) is illustrated for the precipitate located at the pits formed in a bicarbonate buffer (Figure 6). Three characteristic peaks are observed at 221, 434 and 510 cm^{-1}. The peaks at 434 and 510 cm^{-1} have been assigned respectively to the Fe^{2+}—OH and Fe^{3+}—OH stretching modes of green rust [20]. The ratio of the intensity of the Fe(II)—OH/Fe(III)—OH is close to unity and suggests an equal distribution of the hydroxyl ions to Fe(II) and Fe(III), in agreement with the recently published Mössbauer and Raman data obtained from green rust mineral samples [28]. Green rust can also contain CO$_3^{2-}$ species [21] or chloride ions [26]. In the present work, the peak observed at 221 cm^{-1} is linked to the presence of chlorides as nonhydroxyl anions. Moreover, no difference was observed in the shape or location of the symmetrical stretching vibrations of CO$_3^{2-}$ (1065 cm^{-1})

and HCO$_3^-$ (1015 cm^{-1}). This is consistent with the fact that chloride ions are involved instead of CO$_3^{2-}$/HCO$_3^-$ species in the structure of the green rust despite the fact that carbonate green rust as a corrosion product has been reported several years ago [31]. In the latter reference, it is mentioned that the green rust had been obtained through the natural corrosion of water pipes but the experimental conditions remain unclear.

The assignment of the Fe^{2+}—OH and Fe^{3+}—OH stretching modes is confirmed by the Raman spectrum obtained in the solvent D$_2$O (Figure 7). After the formation of green rust in D$_2$O containing NaHCO$_3$ and NaCl, the peaks are shifted to lower frequencies (i.e., 13 cm^{-1}) for the peak Fe^{3+}—OD and 16 cm^{-1} for Fe^{2+}—OD; these values are consistent with the mass increase when the OH groups are replaced by OD groups according to the following equation:

$$\nu_{OD} = \nu_{OH} \sqrt{\frac{m_{OH}}{m_{OD}}}$$

Figure 8 presents the spectrum of the corrosion product obtained in the presence of both the bicarbonate and sulfate anions but free of chloride. The spectrum shows two strong peaks of hydroxyl groups of green rust (433 and 509 cm^{-1}) and another one at 982 cm^{-1}; this very strong and sharp peak is from the symmetrical stretching of the free sulfate ions in solution [33]. The weak bands, originating from symmetric stretching modes of HCO$_3^-$ and CO$_3^{2-}$ in solution, occur at 1015 and 1065 cm^{-1} [34]. A small peak located at 930 cm^{-1} is probably linked to the shift to lower frequency of the stretching mode of the sulfate group when complexed in the solid state [35]. It is concluded that the green rust,
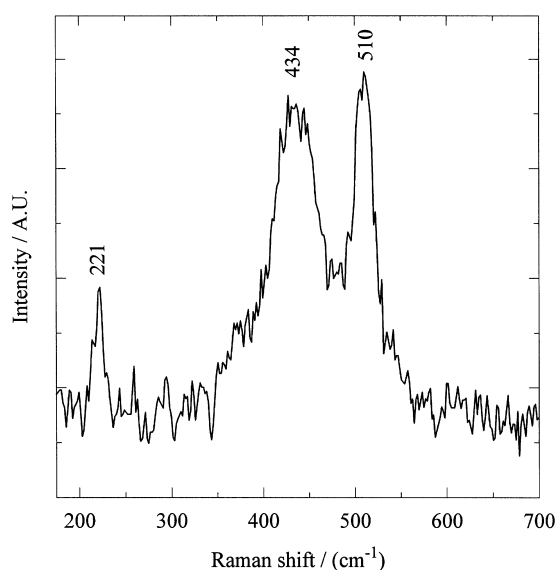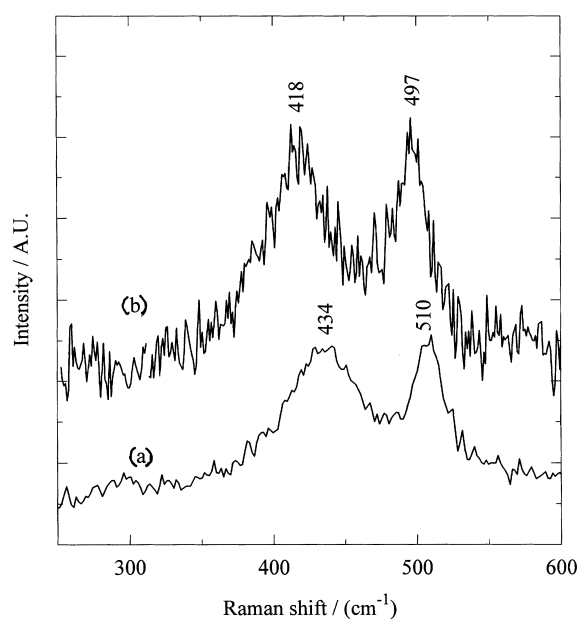
Fig. 6. In situ Raman spectra of the precipitate covering a pit formed on a rotating electrode in deaerated 0.1 M NaHCO$_3$ and 0.15 M NaCl.

Fig. 7. In situ Raman spectra of the precipitate covering a pit formed on a stationary electrode in deaerated 1.0 M NaHCO$_3$ and 0.15 M NaCl for (a) in H$_2$O and (b) in D$_2$O.
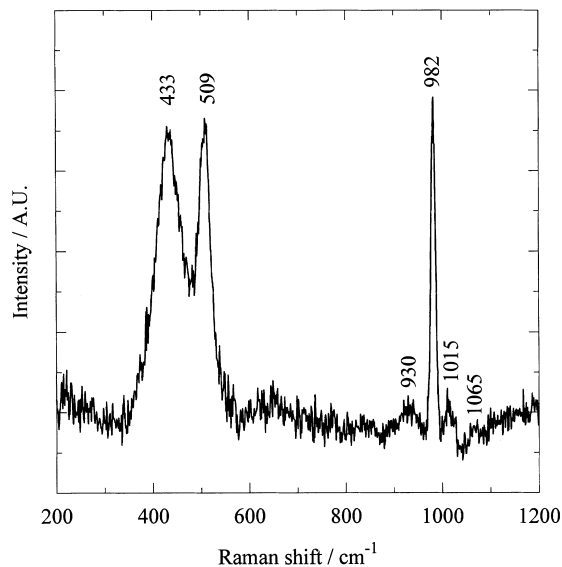
Fig. 8. In situ Raman spectra of the precipitate covering a pit formed on a rotating electrode in deaerated 0.1 M NaHCO₃ + 0.1 M Na₂SO₄.

generated during the localized attack by ions in bicarbonate + sulfate solution, contains sulfate ions as nonhydroxyl anions.

When localized attack is observed in a bicarbonate solution containing both sulfate and chloride ions, the Raman peaks of green rust are still detected (Figure 9). The presence of the peak ascribed to complexed chloride ions and sulfate ions is noticed. The Figure 9 inset reveals the presence of a sulfate peak at 927 cm^{-1}, suggesting that the green rust produced in this solution is a mixture of sulfate and chloride green rust.

Figure 10(a) is the Raman spectrum, recorded *in situ*, of the precipitate covering a pit formed on a rotating
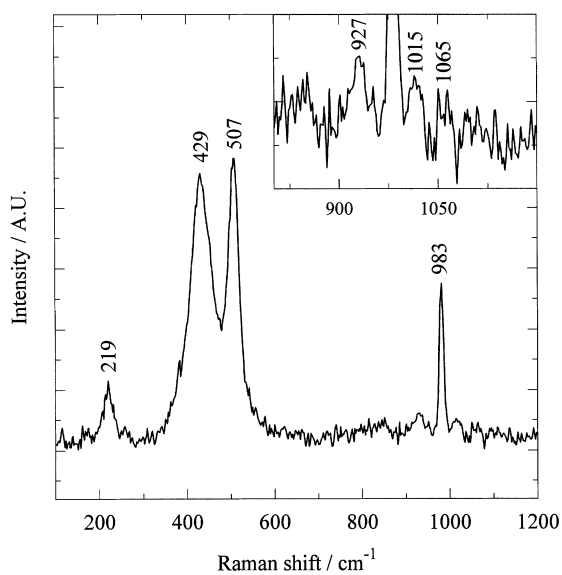

Fig. 9. In situ Raman spectra of the precipitate covering a pit formed on a rotating electrode in deaerated 0.1 M NaHCO₃ + 0.1 M Na₂SO₄ + 0.15 M NaCl.
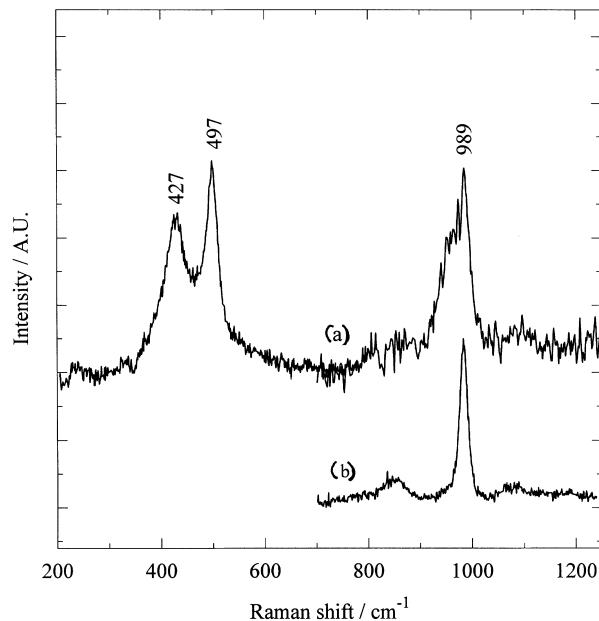

Fig. 10. In situ Raman spectra of: (a) the precipitate covering a pit formed on a rotating electrode in deaerated 0.1 M Na₂HPO₄ + 0.15 M NaCl; (b) a 0.1 M Na₂HPO₄ + 0.15 M NaCl solution.

electrode in contact with a solution containing 0.1 M Na₂HPO₄ and 0.15 M NaCl. The bands at 427 and 497 cm^{-1} arise from M^{n+}—OH stretching modes of green rust, as previously discussed. Chloride is virtually absent in the precipitate, as judged from the intensity at 221 cm^{-1}. The remaining bands arise from phosphate species. For comparison, the spectrum of the electrolyte is presented in Figure 10(b). The hydrogen phosphate anion has symmetric stretching modes at 850 and 987 cm^{-1} [36]. The antisymmetric stretching mode gives a weak band at 1080 cm^{-1}. These three bands are clearly seen in Figure 10(b). Two other deformation modes have weak Raman bands at 530 and 390 cm^{-1} [36]. The phosphate anion has four Raman-active bands [36]: 935 cm^{-1}, P–O symmetric stretch, intense; 1007 cm^{-1}, P–O antisymmmetric stretch, weak; 550 cm^{-1}, deformation, weak; 412 cm^{-1}, deformation, weak. Figure 10(b) shows that the electrolyte contains only a small amount of PO₄$^{3-}$; the evidence is the weak foot on the 989 cm^{-1} band.

The 850, 989 and 1080 cm^{-1} bands of HPO₄$^{2-}$ in the electrolyte show up in Figure 10(a). The deformation bands are masked by the intense M^{n+}—OH bands. However, the low frequency shoulder of the 989 cm^{-1} band – about 935 cm^{-1} – can definitely be assigned to phosphate anion. Its relative height and marked width suggests that it exists in the green rust; it appears to be favoured over the chloride ion. Interestingly, the intensity ratio of the M^{n+}—OH peaks, I₄₂₇/I₄₉₇, is markedly less than unity; this suggests the depletion of OH groups associated to Fe^{2+}; they possibly have extracted the proton from HPO₄$^{2-}$, thereby creating PO₄$^{3-}$. The composition of green rust is seen to be dependent on the nonaggressive anion.

The difference in the composition of green rust accounts for the observed different electrochemical behavior: the green rust generated in bicarbonate solution containing aggressive chloride or sulfate anions may allow mass transfer of dissolved species through its structure; green rust generated in phosphate solution contains nonaggressive PO_4^{3-}/HPO_4^{2-} anions and seems to have an inhibitive effect on the corrosion process by slowing down the growth of the pits. In the latter case, a role of physical barrier can be suggested or a chemical contribution is suggested; however, it is not possible now to discriminate between the two possible contributions. The presence of both chloride and sulfate ions in the hydrogen phosphate solution does not alter this conclusion. The band attributed to phosphate at 935 cm^{-1} is still present (Figure 11). The spectrum does not permit a clear discrimination between sulfate and hydrogen phosphate; both contribute to the line at 983 cm^{-1}. The absence of intensity at about 221 cm^{-1} supports the conclusion that chloride is not a component of this green rust. The precipitate could contain both sulfate and phosphate. Bands at 236 and 327 cm^{-1} may arise from Fe-sulfate of Fe-phosphate modes of vibration.

4. Conclusion

For bicarbonate solution, the green rust generated in the presence of chloride anions contains chloride; no carbonate species are included in its structure. In phosphate media, green rust obtained in the chloride-containing solution also has been identified and the nonhydroxyl ion is a phosphate group. The assignment to the hydroxyl groups contained in green rust has been confirmed by deuterium/hydrogen isotope substitution
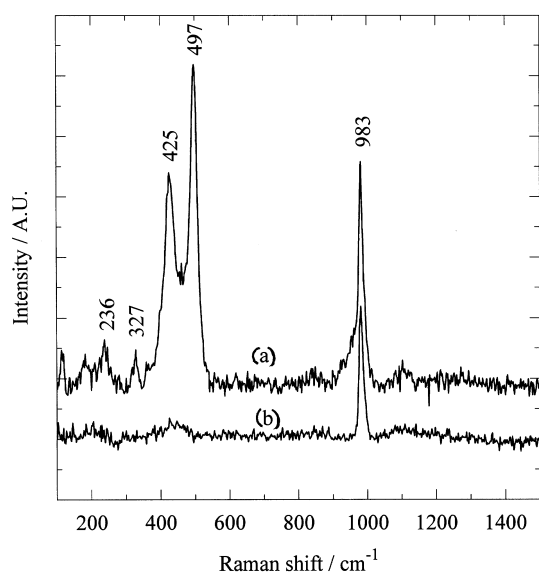

Fig. 11. In situ Raman spectra of the: (a) precipitate covering a pit formed on a rotating electrode in deaerated 0.1 M Na$_2$HPO$_4$ + 0.1 M Na$_2$SO$_4$ + 0.15 M NaCl. (b) Solution of 0.1 M Na$_2$HPO$_4$ + 0.1 M Na$_2$SO$_4$ + 0.15 M NaCl.

and Raman spectroscopy. For the green rust generated in the bicarbonate solution, with sulfate as aggressive anions, the presence of sulfate green rust is suggested. When both chloride and sulfate ions are present, the composition of green rust is most likely a mixture of chloride green rust and sulfate green rust. In the phosphate buffer, no localized attack is observed when sulfate ions are present (without chloride ions). The addition of chloride ions is necessary to induce pitting but the presence of chloride ions in the green rust precipitate is discarded.

The different post-breakdown electrochemical behaviours and the difference in the morphology of the precipitate for the electrodissolution of mild steel is most likely linked to the two different compositions of the green rust obtained from different solutions. The phosphate green rust may act as a physical barrier preventing the aggressive anions ingress inside the pit or have a chemical inhibition effect. As far as the chloride green rust is considered, ingress of solution species inside the pit is possible through its structure.

References

1. J.R. Galvele, *in* R.P. Frankenthal and J. Kruger (Eds), '*Passivity of Metals*', The Electrochemical Society, Pennington, NJ (1978), p. 285.
2. J.R. Galvele, *in* J.C. Scully (Ed), 'Treatise on Materials Science and Technology', Vol. 23, '*Corrosion: Aqueous Processes and Passive Films*' (Academic Press, London, 1983), pp. 1–57.
3. Z. Szklarska-Smialowska, *in* '*Pitting Corrosion of Metals*' (NACE. Houston TX 1986).
4. E.B. Castro C, C.R. Valentini, C.A. Moina, J.R. Vilche and A.J. Arvia, *Corros. Sci.* **26** (1986) 781.
5. P. Southworth, A. Hamnett, A.M. Riley and J.M. Sykes, *Corros. Sci.* **28** (1988) 1139.
6. J.G.N. Thomas, T.J. Nurse and R. Walker, *Br. Corros. J.* **5** (1970) 87.
7. R.D. Armstrong and A.C. Coates, *Electroanal. Chem Interf. Electrochem.* **50** (1974) 303.
8. S. Simard, M. Drogowska, L. Brossard and H. Ménard, *J. Appl. Electrochem.* **27** (1997) 317.
9. N. Sato, T. Noda and K. Kudo, *Electrochim. Acta* **19** (1974) 471.
10. N. Sato, K. Kudo and T. Noda, *Z. Physik. Chem. N. F.* **98** (1975) 271.
11. Z. Szklarska-Smialowska and R.W. Staehle, *J. Electrochem. Soc.* **121** (1974) 1393.
12. K. Tonkunaga, *Jap. J. Appl. Phys.* **21** (1982) 1693.
13. K. Ogura, A. Fujishima, Y. Nagae and K. Honda, *J. Electroanal. Chem.* **162** (1984) 241.
14. R. Nishimura and K. Kudo, *Surf. Sci.* **96** (1980) 413.
15. (27) 27-C. A. Melendres, N. Camillone III and T. Tipton, *Electrochim. Acta* **34** (1989) 281.
16. M. Ergun and A.Y. Turan, *Corros. Sci.* **32** (1991) 1137.

17. M. Cohen, *Corros.* **32** (1976) 461.
18. S. Simard, L. Brossard and H. Ménard, *J. Appl. Electrochem.* **28** (1998) 523.
19. S. Simard, L. Brossard and H. Ménard, *J. Appl. Electrochem.* **28** (1998) 151.
20. N. Boucherit and A. Hugot-Le Goff, *Faraday Discuss.* **94** (1992) 137.
21. H.C.B. Hansen, *Clay Miner.* **24** (1989) 663.
22. S.H. Drissi, Ph. Refait, M. Abdelmoula and J.M.R. Génin, *Corros. Sci.* **37** (1995) 2025.
23. J.M.R. Génin, D. Rézel, P. Bauer, A.A. Olowe and A. Béral, *Mater. Sci. Forum* **8** (1986) 477.
24. J.M.R. Génin, P. Bauer, A.A. Olowe and A. Béral, *Hyperfine Interact*. The Netherlands **29** (1986) 1355.
25. Ph. Refait and J.-M.R. Génin, *Corros. Sci.* **36** (1994) 55.
26. Ph. Refait and J.-M.R. Génin, *Corros. Sci.* **34** (1993) 797.
27. Y. Tamaura, *Inorg. Chem.* **24** (1985) 4363.
28. F. Trolard, J.-M. R. Génin, M. Abdelmoula, G. Bourrié, B. Humbert and A. Herbillon, *Geochim. Cosmochim. Acta* **61** (1997) 1107.
29. I.R. McGill, B. McEnaney and D.C. Smith, *Nature* **259** (1976) 200.
30. P.M.L. Bonin, M.S. Odziemkowski, G.J. Reardon and R.W. Gillham, *J. Sol. Chem.* **39** (2000) 1061.
31. M. Ergun and A.Y. Turan, *Corros. Sci.* **32** (1991) 1137.
32. P.P. Stampfs, *Corros. Sci.* **9** (1969) 185.
33. B.S.W. Dawson, D.E. Irish and G.E. Toogood, *J. Phys. Chem.* **90** (1986) 334.
34. A.R. Davis and B.G. Oliver, *J. Solution. Chem.* **1** (1972) 329.
35. K. Nakamoto, *in 'Infrared and Raman Spectra of Inorganic and Coordination Compounds'*, 4th edn. (Wiley-Interscience, New York, 1986).
36. C.M. Preston and W.A. Adams, *J. Phys. Chem.* **83** (1979) 814; *Can. J. Spectrosc.* **22** (1977) 125.